



OPEN Study on mechanical properties and acoustic emission evolution law of raw coal in water-mechanical coupling environment

Jingke Wu¹, Fuxing Xie²✉ & Yushun Yang³

This study addresses the critical issue of water-coal interaction in deep coal mining, which affects safe and efficient production. Taking raw coal samples from the Wu Group of Pingmei No. 11 Mine as the research object, uniaxial compression and acoustic emission monitoring tests were conducted under different water immersion times (0 h, 4 h, 8 h, 12 h, 24 h, 48 h). The mechanical properties, deformation and failure behaviors, and energy evolution patterns of water-bearing coal samples were systematically investigated. The results show that the stress-strain relationship curves of coal samples with different moisture contents exhibit four distinct stages: the crack compaction stage, the linear elastic stage, the plastic deformation stage, and the post-peak failure stage. With increasing moisture content, the failure morphology of the curves transitions from brittle to ductile. The elastic modulus, deformation modulus, and peak strength of the coal samples decrease significantly following a quadratic function with increasing moisture content, while the softening coefficient increases in a quadratic function form. Acoustic emission activity can be divided into three stages: a quiet period, a slow increase period, and a sharp increase period, which correspond to the crack compaction stage, the linear elastic stage, and the yield-failure stage in the stress-strain process, respectively. Analysis based on the energy dissipation theory indicates that only a small portion of the energy absorbed by coal samples during compression is stored as elastic energy, while most of the energy is dissipated in irreversible processes such as pore compaction, crack sliding, and crack propagation. Both the total absorbed energy and the releasable elastic energy before the peak decrease in a quadratic function form with increasing moisture content. This study provides important experimental evidence and a theoretical reference for the stability evaluation and disaster prevention and control of deep water-bearing coal masses.

Keywords Water-bearing of raw coal, Uniaxial compression, Mechanical properties, Acoustic emission properties, Energy properties

Coal, as a vital energy source, holds a dominant position in China's energy structure. As coal mining progressively extends to greater depths, the conditions for extraction become increasingly complex, and the interaction between water and coal masses has a growing impact on the safety production of coal mines¹⁻³. Long-term engineering practices both domestically and internationally have confirmed that coal seam water infusion, as a prevention and control technical measure⁴⁻⁷, can effectively mitigate dynamic coal-rock disasters, gas outbursts, coal dust hazards, and other risks at their source. This measure (coal seam water infusion) significantly influences the mechanical, energetic, and acoustic emission characteristics of coal masses, thereby providing crucial support for the safety production of coal mines.

Due to the presence of moisture, the mechanical, energy, and acoustic emission properties of water-bearing coal samples differ markedly from those of dry samples. Scholars worldwide have conducted extensive research on water-bearing coal samples, laying a theoretical foundation for a deeper understanding of coal mass behavior and providing support for the safety production of coal mines. Regarding the mechanical properties of coal samples, studies have focused on the effect of moisture on parameters such as strength and elastic modulus. Zhang, J.J.⁸ et al. observed that the uniaxial compressive strength of coal samples decreases significantly with increasing

¹School of Intelligent Manufacturing and Smart Transportation, Suzhou City University, Suzhou 215104, China.

²Beijing China Coal Mine Engineering Co., Ltd., Beijing 100013, China. ³State Key Laboratory of Coking Coal Exploitation and Comprehensive Utilization, Pingdingshan 467000, China. ✉email: fxxcmt@126.com

moisture content, indicating a weakening effect of water on coal structure. Yang, K⁹ et al. reported that the elastic modulus decreases linearly with rising moisture content, with saturated samples showing a 41.2% reduction compared to dry samples, which is consistent with the mechanism by which water weakens the cementation between particles. Zhang, M.B¹⁰ et al. found that higher moisture content leads to lower triaxial strength in coal samples, faster loss of resistance to failure caused by external loads, enhanced plastic deformation, reduced brittle failure, and smaller increases in gas flow rate. Wang, B.F¹¹ et al. analyzed the relationship between internal fabric characteristics and macroscopic mechanical properties of coal-rock blocks. Their study revealed that, compared with natural coal-rock samples, saturated ones exhibit significant changes in strain and swelling coefficient. Li, B.B¹² et al. noted that with increasing moisture content, the peak stress of coal rock decreases due to the action of water, and Poisson's ratio increases, while the elastic modulus decreases linearly and monotonically, resulting in a gradual reduction in brittleness. Yao, Q.L¹³ et al. found that as water saturation increases, the uniaxial compressive strength, elastic modulus, and internal friction angle of coal-bearing rocks decrease linearly or exponentially, while the cohesion decreases exponentially. Duan, S.L¹⁴ et al. investigated the permeability evolution of water-bearing coal rock under the combined effects of effective stress and dynamic slip effects. At the constant moisture content, permeability decreases exponentially with increasing effective stress; at constant effective stress, higher moisture content leads to lower permeability. Yin, D.W^{15,16} et al. reported that the uniaxial compressive strength and elastic modulus of pressure-water-soaked coal samples are negatively correlated with the initial damage amount. Compared with dry samples, the uniaxial compressive strength of pressure-water-soaked samples after cyclic loading and unloading decreased by 18.04%, 27.12%, and 42.82%, respectively. Chen, J.X¹⁷ et al. analyzed the corrosion characteristics and dynamic properties of coal-rock combinations under hydrochemical conditions, noting that the dynamic compressive strength of samples in the same solution decreases continuously with increasing immersion time, while samples in acidic solutions exhibit stronger time dependence. Chen, G.B¹⁸ et al. suggested that under cyclic water immersion, repeated physical, chemical, and mechanical interactions between water and rock cause cumulative damage to coal rock, ultimately leading to the deterioration of macroscopic mechanical properties. Lü, K¹⁹ et al. found that the deterioration effect of water and gas alters the internal pore structure of coal samples. The destruction of the original supporting structure of coal samples in a soaked environment reduces their ability to store energy before failure. Gao, M.Z²⁰ et al. observed that water causes the micro-surface of coal to peel off and cracks to expand and develop. With increasing soaking time, the uniaxial and triaxial strengths of coal samples decrease nonlinearly, with a decrease of 63.31% and 30.95% after 240 h of soaking, respectively. Qi, X.H^{21,22} et al. found that with increasing moisture content, the mesoscopic damage of coal masses intensifies, and the axial peak strain, peak strength, and elastic modulus gradually decrease, while Poisson's ratio gradually increases. Li, S.W²³ et al. conducted dynamic mechanical experiments on coal rocks under saturated conditions at various depths, concluding that under various depth conditions, the dynamic strength of coal in a saturated state decreases compared to that in the natural state of coal. Ma, Y.K²⁴ et al. performed experiments on coal-rock fracturing via high-pressure air impact under water coupling, finding that water coupling significantly improves the energy utilization efficiency of high-pressure air, resulting in noticeably longer horizontal and vertical cracks in test blocks compared to those under air coupling. Pi, Z.K²⁵ et al. reported that as soaking cycles increase, the porosity of coal samples treated with continuous high-pressure soaking and high-low pressure cyclic soaking first decreases slightly and then increases gradually. Feng, R.J^{26,27} et al. analyzed the damage and failure characteristics of loaded coal rocks under high-pressure pulsed water jet impact, revealing the influence of key parameters such as the average velocity of the water jet, pulse amplitude, and pulse frequency on such characteristics.

Based on the above analysis, it is evident that scholars worldwide have conducted extensive research on the deformation and mechanical properties of water-bearing coal samples and have obtained a series of important findings. However, studies on the energy and acoustic emission characteristics of water-bearing coal samples are relatively scarce. Given the complex and variable occurrence environments of coal masses, this paper focuses on the Wu Group coal from No. 11 Mine of Pingdingshan Tianan Coal Industry Co., Ltd. as the research object. An in-depth study of the mechanical, deformational, energetic, and acoustic emission characteristics of raw water-bearing coal samples under uniaxial compression has significant theoretical and engineering value for revealing the mechanisms behind dynamic coal-rock disasters and formulating scientific and effective disaster prevention measures.

Sample equipment, sample preparation, and research plan

Experimental apparatus

The testing machine employed was the “TAW-600 Electro-Hydraulic Servo Coal Rock Uniaxial Compression Testing Machine,” as shown in Fig. 1(a). This machine is capable of collecting data such as stress, displacement, and time. The acoustic emission system utilized a PCI-2 fully digital acoustic emission monitoring instrument, which can simultaneously record parameters including amplitude, energy, ring-down count, rise time, and RMS voltage, and generate correlation diagrams of these parameters. The acoustic emission probes were of the model NANO-30, installed on the side surfaces of the specimens. A small amount of Vaseline was applied between the probes and the specimens to serve as a coupling agent, thereby reducing signal attenuation. The sampling frequency was set to 1 MHz, and the preamplifier gain was set to 40 dB. After the specimen installation was completed, the acoustic emission monitoring system and the testing machine loading system were started simultaneously.

Coal sample Preparation

The specimens were obtained from the Wu Group coal seam of Pingmei No. 11 Mine. Large coal blocks with initial dimensions exceeding 200 mm were collected on-site and transported to the laboratory. Wet coring methods were employed to extract coal cores from these blocks. The ends of the specimens were then cut and

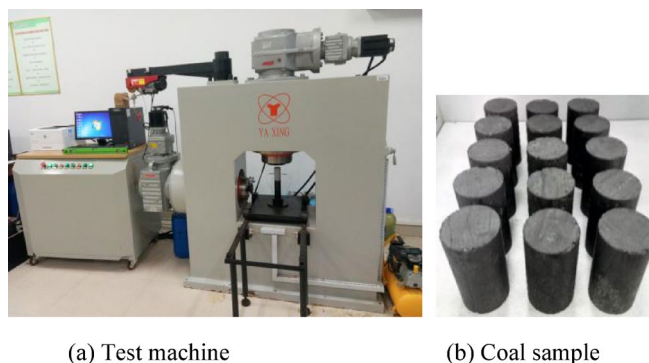


Fig. 1. Test system and test samples.

Immersion time/h	No.	Dry mass/g	Water absorption mass/g	Moisture content/%	Average moisture content/%
0	1#	345.6			0
	2#	349.3			
4	3#	345.2	346.2	0.29	0.25
	4#	346.1	346.8	0.20	
8	5#	351.4	352.6	0.34	0.30
	6#	353.2	354.1	0.25	
12	7#	355.4	357.2	0.51	0.52
	8#	351.3	353.1	0.51	
	9#	349.2	351.1	0.54	
24	10#	351.1	353.5	0.68	0.64
	11#	350.2	352.3	0.6	
48	12#	353.2	355.9	0.76	0.75
	13#	352.1	354.8	0.77	
	14#	354.6	357.2	0.73	

Table 1. Moisture content of coal samples after water immersion.

polished using a cutting machine to fabricate standard cylindrical samples (100 mm in height and 50 mm in diameter). The processing accuracy complied with the requirements specified by standard methods for testing physical and mechanical properties of rocks. A prepared coal sample is shown in Fig. 1(b).

Experimental plan

Coal sample moisture characteristics test

Firstly, the coal samples were placed in a constant-temperature blast drying oven at 60°C for 24 h to ensure complete evaporation of internal moisture. They were then removed and cooled to room temperature in a desiccator before their dry mass was measured. Subsequently, the dried coal samples were fully immersed in an airtight container filled with the soaking solution. Environmental conditions: The entire immersion process was conducted at room temperature ($20 \pm 2^\circ\text{C}$) to maintain constant environmental conditions, and under atmospheric pressure. To ensure full water absorption by the coal samples, the “vacuum saturation method” was applied to those immersed for 12 h or longer. The designated immersion time points were 0 h (dry sample), 4 h, 8 h, 12 h, 24 h, and 48 h. Upon reaching the predetermined time, the coal samples were taken out, and any surface moisture was gently wiped off using a damp towel. Their mass after water absorption was immediately measured to calculate the moisture content of the samples. The test results are presented in Table 1.

Based on the experimental data in Table 1, the relationship curve between the moisture content of coal samples and immersion time was plotted, as shown in Fig. 2.

As shown in Fig. 2, the variation of moisture content in the coal samples with immersion time exhibits a distinct two-stage characteristic: (1) Rapid Increase Stage (0–12 h): During this stage, although the immersion time is relatively short, the water absorption capacity of the coal samples is strong. The moisture content reaches 0.25% after 4 h of immersion, increases at an accelerated rate to 0.30% between 4 and 8 h, and reaches 0.52% at 12 h. This indicates that the open pores and fractures within the coal samples have been completely filled with water during this phase. (2) Slow Increase Stage (12–48 h): In this stage, despite the longer immersion time, the water absorption capacity of the coal samples weakens. The moisture content reaches 0.64% after 24 h and 0.75% after 48 h of immersion. During this phase, the vacuum saturation method is applied to facilitate the penetration of water molecules into the closed pores and fractures inside the coal samples, achieving a forced saturated state.

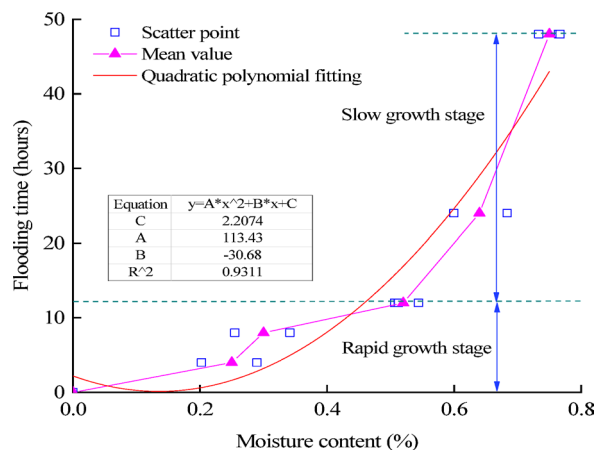


Fig. 2. Relationship curve between immersion time and moisture content.

Uniaxial compression and acoustic emission test of water-bearing coal sample

Place the soaked coal sample into the “TAW-600 Electro Hydraulic Servo Coal Rock Uniaxial Pressure Testing Machine” test bench, attach an acoustic emission probe to the surface of the coal sample, and simultaneously conduct uniaxial compression tests and acoustic emission tests on the coal sample under different moisture content conditions. The uniaxial compression loading rate of the coal sample is set to 0.1 mm/min.

Mechanical and deformation characteristics of water-bearing coal samples

Stress strain relationship curve

Based on the experimental data, draw the axial stress-strain relationship curves of each water-bearing coal sample under different moisture content conditions after uniaxial compression failure, as shown in Fig. 3.

As can be seen from Fig. 3, the axial compression deformation of the coal samples continuously increases with the rising axial pressure. Once the axial pressure reaches a certain level, the coal samples undergo instability and failure, while deformation continues to progress. The stress-strain curves of the coal samples with different moisture contents can be divided into four distinct stages: (1) Crack Compaction Stage: The stress-strain curve exhibits an upward concave nonlinear growth. Under axial loading, the original open cracks gradually close, resulting in volumetric compression of the sample. The deformation in this stage is irreversible and reflects the initial damage degree of the coal mass. (2) Linear Elastic Stage: The stress-strain curve shows a linear relationship, and the volume continues to contract, following Hooke’s law. This stage demonstrates the elastic characteristics of the coal sample. (3) Plastic deformation stage: The stress-strain curve becomes downward concave. Irreversible plastic deformation occurs in the coal sample, accompanied by varying degrees of internal damage. (4) Post-Peak Failure Stage: The axial stress reaches the ultimate bearing capacity of the coal sample. Macroscopic sliding occurs along a certain failure surface inside the specimen, leading to a loss of load-bearing capacity, a rapid drop in stress, and further intensification of deformation. Comparing the curves, it is evident that with increasing moisture content, both the slope of the elastic segment (elastic modulus) and the peak stress point (uniaxial compressive strength) decrease significantly. Moreover, the post-peak curve gradually becomes flatter, indicating that water intrusion not only weakens the strength of the coal mass but also transitions its failure mode from brittle to ductile.

Table 2 shows the deformation parameters of each coal sample under different moisture conditions. In the table, σ_c is the peak strength, E_0 is the initial modulus (taking the slope of the line connecting the 5% peak strength point of the axial stress-strain curve and the origin), E_{50} is the deformation modulus (taking the slope of the line connecting the 50% peak strength point of the axial stress-strain curve and the origin), E is the elastic modulus (taking the slope of the approximately straight line segment of the axial stress-strain curve), and ϵ_c is the peak strain (the axial strain value corresponding to the peak strength).

As can be seen from Table 2, the uniaxial compressive strength (UCS) of the coal samples ranges from 6.9 to 38.55 MPa, and the elastic modulus varies between 1.06 and 4.47 GPa. A clear trend is observed: both the compressive strength and elastic modulus exhibit a decreasing tendency with prolonged immersion time. The average UCS of the dry samples is 36.06 MPa, and the average elastic modulus is 3.93 GPa. At a moisture content of 0.25%, the UCS and elastic modulus decrease by 7.46 MPa and 0.21 GPa, respectively. When the moisture content reaches 0.3%, the UCS decreases by 4.95 MPa, while the elastic modulus increases slightly by 0.13 GPa. At 0.52% moisture content, reductions of 2.87 MPa in UCS and 0.97 GPa in elastic modulus are observed. With a moisture content of 0.64%, the UCS decreases by 3.55 MPa and the elastic modulus by 0.07 GPa. Finally, at 0.75% moisture content, the UCS decreases by 7.07 MPa and the elastic modulus by 0.98 GPa. Compared to the dry state, the total reduction in UCS and elastic modulus reaches 71.82% and 53.44%, respectively. These results clearly indicate that both the elastic modulus and uniaxial compressive strength of the coal samples deteriorate significantly with increasing moisture content. This degradation can be attributed to two main mechanisms: Firstly, the intrusion of water molecules into the pores and fractures of the coal generates pore water pressure, which reduces the effective stress between particles^{13,20}. Secondly, physico-chemical interactions between water

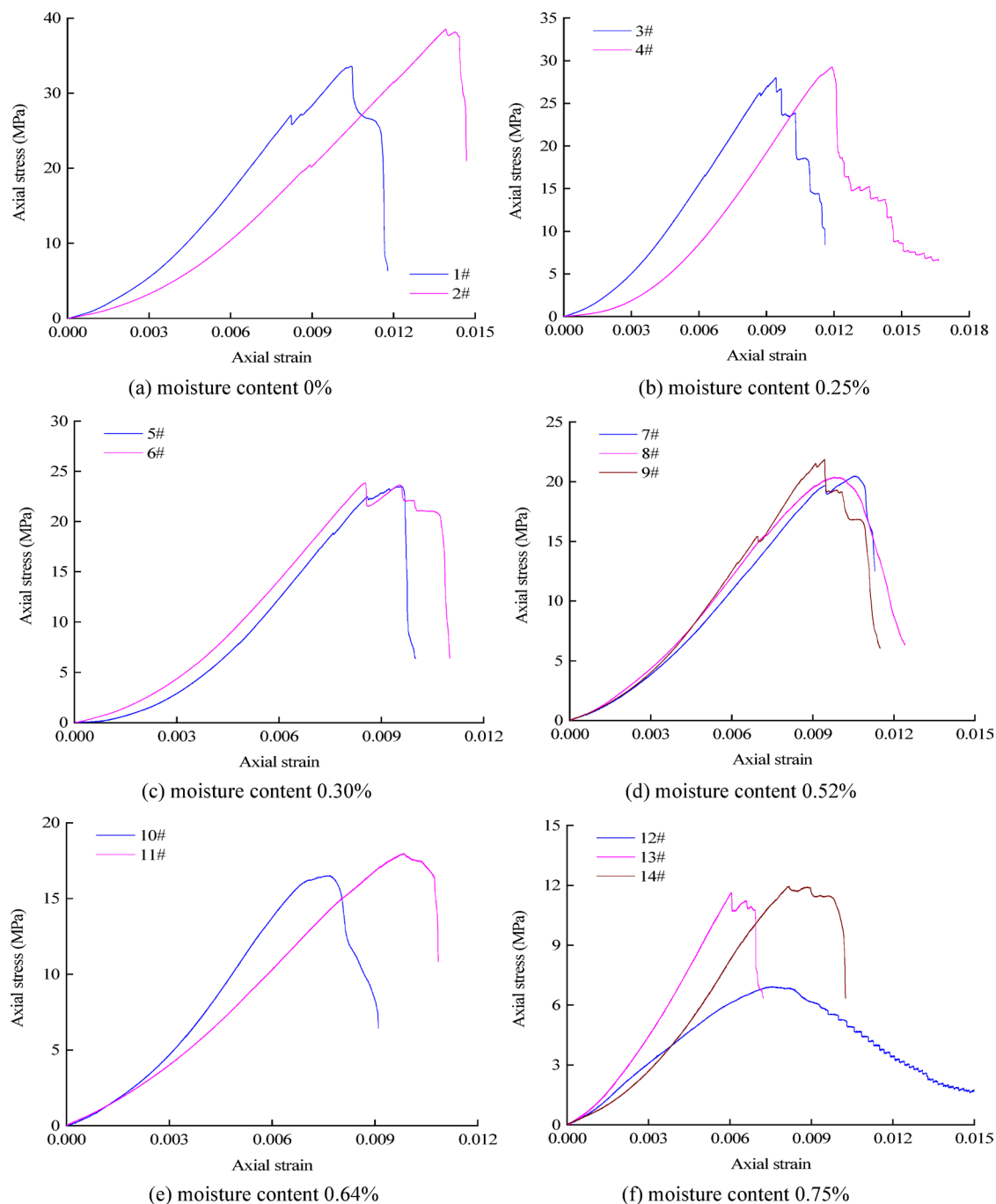


Fig. 3. Stress strain relationship curves of coal samples under different moisture content conditions.

and the coal matrix occur. On one hand, water softens and dissolves clay minerals and other cementing materials within the coal; on the other hand, the wedge action of water promotes the propagation of micro-fractures. These processes fundamentally weaken the internal structure of the coal and reduce the bonding strength between particles^{12,17,28}.

Influence of water on deformation parameters of coal samples

Based on the test data in Table 2, the relationship curve between deformation parameters of the coal sample and the moisture content are plotted, as shown in Fig. 4.

As shown in Fig. 4(a), the average elastic modulus of the coal samples is 3.93 GPa in the dry state. With increasing moisture content, the values are 3.72 GPa at 0.25%, 3.85 GPa at 0.30%, 2.88 GPa at 0.52%, 2.81 GPa at 0.64%, and 1.76 GPa at 0.75%. The elastic modulus is a key parameter for evaluating the elastic deformation characteristics of coal under compression, reflecting the sample's ability to resist deformation and failure. The presence and variation of moisture are primary factors influencing the elastic modulus. During elastic

Immersion time/h	0		4		8			
Moisture content/%	0		0.25		0.30			
Coal sample	1#	2#	3#	4#	5#	6#		
σ_c /MPa	33.56	38.55	27.99	29.21	23.49	23.8		
E_0 /GPa	1.02	0.91	1.09	0.55	0.74	0.94		
E_{50} /GPa	2.78	2.25	2.49	1.88	2.01	2.2		
E /GPa	4.47	3.38	3.81	3.62	3.94	3.75		
Peak strain/ 10^{-3}	10.48	13.94	9.43	11.9	9.59	8.53		
Immersion time/h	12		24		48			
Moisture content/%	0.52		0.64		0.75			
Coal sample	7#	8#	9#	10#	11#	12#	13#	14#
σ_c /MPa	20.43	20.4	21.5	16.5	17.9	6.9	11.6	12
E_0 /GPa	0.93	0.96	0.95	1.84	1.88	2.96	1.73	1.39
E_{50} /GPa	1.78	1.9	1.97	1.95	1.66	1.03	1.57	1.24
E /GPa	2.66	2.94	3.05	1.62	1.92	2.35	1.54	1.39
Peak strain/ 10^{-3}	10.6	10	9.44	7.69	9.8	7.69	6.02	8.06

Table 2. Deformation parameters of each water containing coal sample.

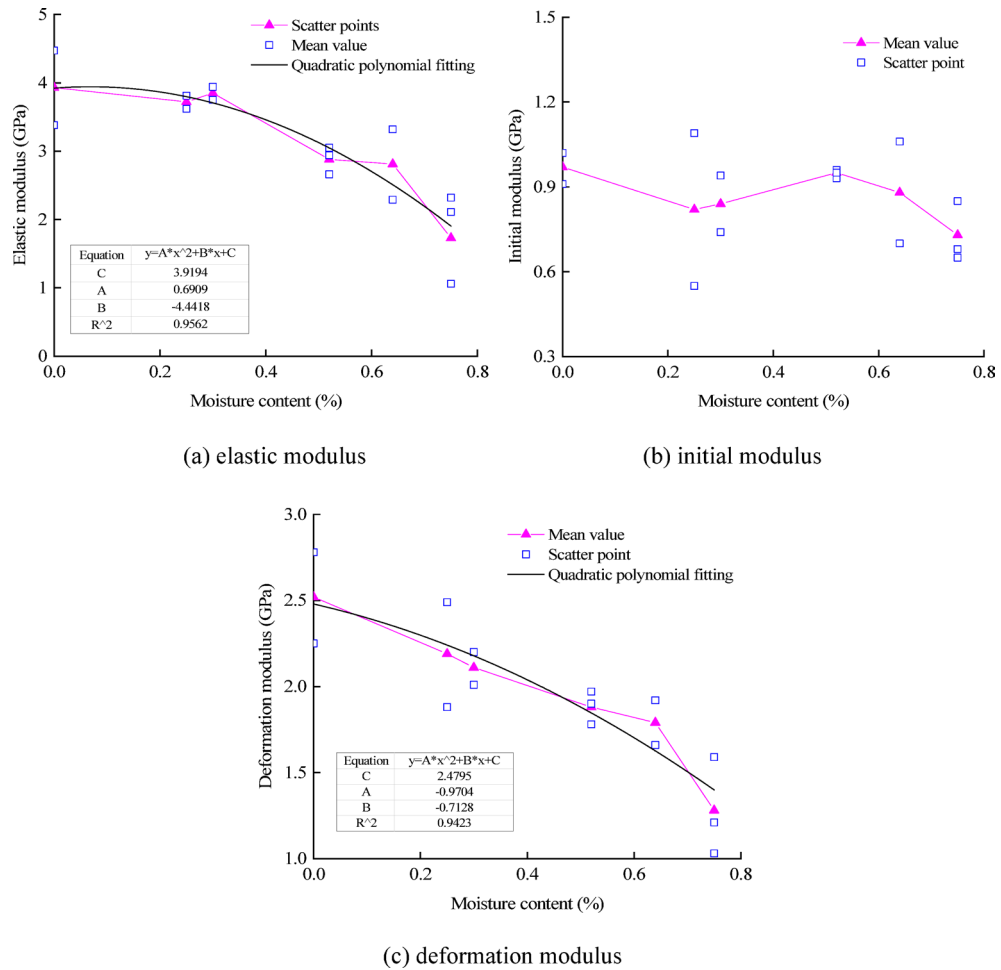


Fig. 4. Relationship curve between deformation parameters and moisture content of coal sample.

deformation, water induces changes in the internal structure and facilitates the movement of fractures and pores, significantly reducing internal friction. This effect allows the sample to undergo larger deformations under relatively lower loads, diminishing its resistance to deformation and failure, and consequently reducing the elastic modulus. As the moisture content increases, the elastic modulus decreases following a quadratic function.

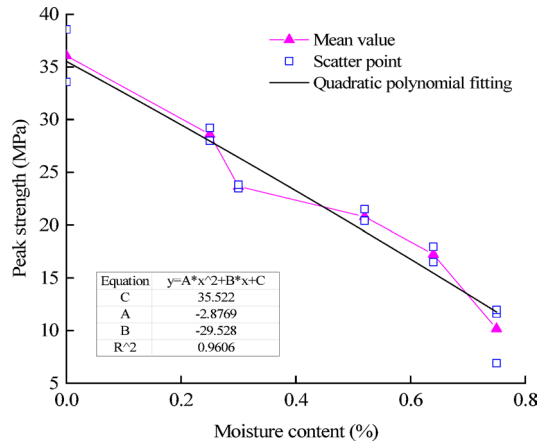
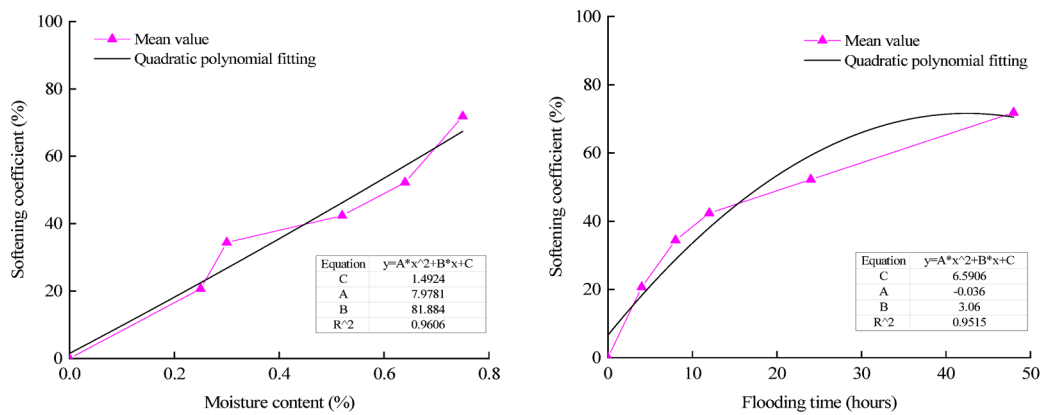


Fig. 5. Uniaxial compressive strength variation curve with moisture content.



(a) Softening coefficient variation curve with moisture content (b) Softening coefficient variation curve with infiltration time

Fig. 6. Softening coefficient and moisture content, softening coefficient and infiltration time relationship curve.

From Fig. 4(b), the initial modulus of the coal sample in the dry state is 0.97GPa. The average initial modulus is 0.82GPa when the moisture content is 0.25%, 0.84GPa when the moisture content is 0.30%, 0.95GPa when the moisture content is 0.52%, 0.88GPa when the moisture content is 0.64%, and 0.73GPa when the moisture content is 0.75%. The initial modulus of coal samples shows a fluctuating change of first decreasing, then increasing, and then decreasing again with the increase of moisture content. As observed in Fig. 4(c), the deformation modulus of the coal sample in the dry state is 2.52GPa. The average deformation modulus is 2.19GPa when the moisture content is 0.25%, 2.11GPa when the moisture content is 0.30%, 1.88GPa when the moisture content is 0.52%, 1.79GPa when the moisture content is 0.64%, and 1.28GPa when the moisture content is 0.75%. As the moisture content of the coal sample increases, the initial modulus of the coal sample decreases as a quadratic function.

Effect of water on the mechanical properties of coal samples

Based on the test data in Table 2, the relationship curve between the peak strength of coal samples and moisture content is plotted, as shown in Fig. 5.

As shown in Fig. 5, the uniaxial compressive strength (UCS) of the coal samples is 36.06 MPa in the dry state. With increasing moisture content, the UCS values are 28.60 MPa at 0.25%, 23.65 MPa at 0.30%, 20.78 MPa at 0.52%, 17.20 MPa at 0.64%, and 10.17 MPa at 0.75%. As the moisture content rises, the UCS decreases according to a quadratic function.

The above analysis indicates that water reduces the strength of coal samples, which is attributed to the softening effect of water. This effect can be quantified using the “softening coefficient,” defined as the ratio of the UCS of saturated coal samples to that of dry samples. A higher softening coefficient indicates better water resistance of the coal. Based on the experimental results, the relationship curves between the softening coefficient and moisture content, as well as between the softening coefficient and immersion time, are plotted in Fig. 6. It can be observed that the softening coefficient increases in a quadratic manner with rising moisture content. During the immersion process, the interaction between water and coal is particularly strong. The softening coefficient

reaches 20.69% after 4 h of immersion and increases to 71.82% after 48 h, demonstrating relatively strong water resistance. As immersion time continues, the softening coefficient also increases following a quadratic function.

Acoustic emission characteristics of water-bearing coal samples

Based on the analysis of experimental data, the relationship curves of stress, time, acoustic emission ring-down count, and cumulative ring-down count during the uniaxial compression failure process of coal samples with various moisture contents are shown in Fig. 7.

The acoustic emission characteristics of coal samples can reflect their internal micro-failure activities and are closely related to internal defects. The acoustic emission behavior and damage deformation characteristics of coal samples with different moisture contents under various failure modes can be described using the ring-down count. As shown in Fig. 7, the cumulative ring-down count of coal samples under different immersion times exhibits distinct stage-wise variations. With increasing loading time, the acoustic emission process of coal samples can be divided into three stages: a quiet period, a slow increase period, and a rapid increase period.

The quiet period occurs during the initial loading stage, characterized by an extremely low ring-down count rate, a flat curve, and slow growth in the cumulative count. This stage corresponds to the initial compaction process of the coal sample, where external load primarily overcomes the closure of inherent pores and micro-fractures without initiating new damage. In samples with longer immersion times, the softening effect of water facilitates easier closure of original fractures, potentially shortening the duration of the quiet period. The slow increase period corresponds to the elastic deformation stage. The ring-down count begins to rise, and the cumulative curve shows an increasing trend, indicating gradually intensifying micro-fracturing activities. During this stage, the coal sample undergoes elastic deformation, and local stress concentrations lead to the initiation and stable propagation of new fractures, though no macroscopic failure surface has yet formed. In samples with higher moisture content, the lubricating effect of water molecules reduces fracture propagation resistance, potentially resulting in a higher increase in ring-down count compared to dry samples. The rapid increase period corresponds to the plastic deformation and instability failure stage. The ring-down count surges, and the cumulative curve exhibits a “steep rise” pattern, typically reaching its maximum near the peak stress. During this stage, internal fractures coalesce to form macroscopic shear bands or tensile failure surfaces, accompanied by intense energy release, leading to an explosive growth in acoustic emission signals. The weakening effect of moisture causes high-moisture coal samples to enter the instability stage earlier, but the total cumulative ring-down count may decrease due to the reduced strength of the coal mass (compared to dry samples).

Energy evolution characteristics of water-bearing coal samples

Energy calculation principle

The deformation and failure process of coal samples is essentially an energy driven process, involving the input of external mechanical work, the storage of internal elastic properties, and the release of dissipated energy. Based on the first law of thermodynamics (conservation of energy), the energy evolution process of water containing coal samples in uniaxial compression tests can be quantitatively described as follows^{29,30}:

$$U = U^d + U^e \quad (1)$$

In the formula, U is the total energy input by the testing machine; U^d is dissipated energy (irreversible energy loss such as plastic deformation and crack propagation); U^e is the releasable elastic strain energy, with a dimension of MJ/m^3 .

Figure 8 shows the relationship curve between dissipated energy and releasable elastic energy during uniaxial compression of coal samples. The total energy input to the water containing coal sample by the testing machine is the area under the stress-strain curve.

$$U = \int_0^{\varepsilon_f} \sigma d\varepsilon_1 \quad (2)$$

The integral in Eq. (2) is calculated by summing the area of small trapezoidal blocks using stress-strain curves:

$$U = \sum_{i=1}^n \frac{\sigma_i + \sigma_{i-1}}{2} (\varepsilon_i - \varepsilon_{i-1}) \quad (3)$$

In the formula, n is the number of sampling points for the stress-strain curve; i is the i -th sampling point; σ_i and ε_i are the stress and strain at point i , respectively.

The elastic energy U^e that can be released can be calculated using the area of the triangle enclosed by BCD:

$$U^e = \frac{1}{2} \frac{\sigma_1^2}{E_T} \quad (4)$$

Due to the approximate linearity of stress-strain in the pre-peak stage, the unloading modulus E_T is replaced by the elastic modulus E . The dissipated energy is the difference between the total energy and the elastic energy:

$$U^d = \int_0^{\varepsilon_f} \sigma d\varepsilon_1 - \frac{\sigma_1^2}{2E_T} \quad (5)$$

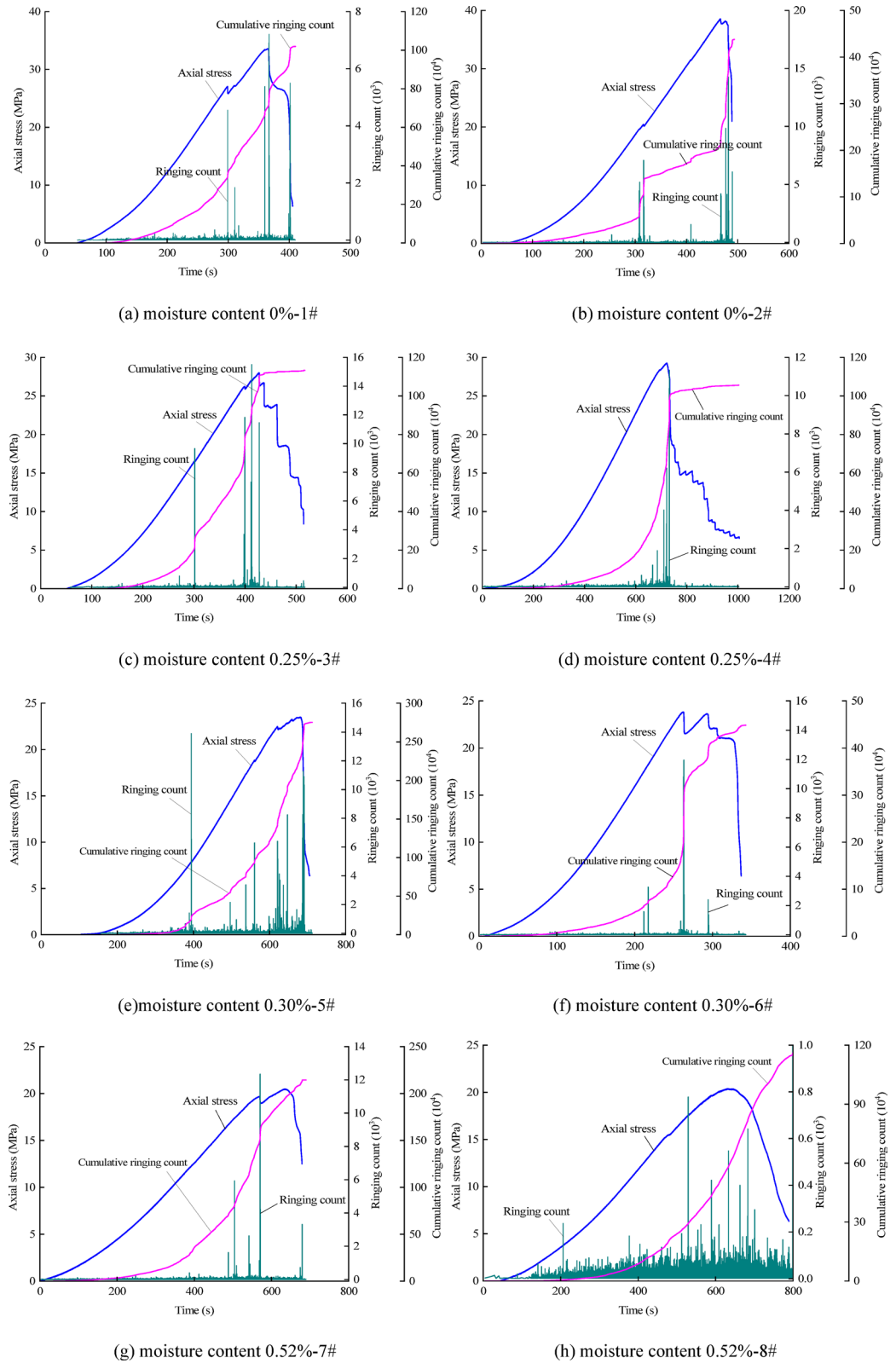


Fig. 7. Curves of stress-time-ringdown count and stress-time-cumulative count of each coal sample under different moisture content conditions.

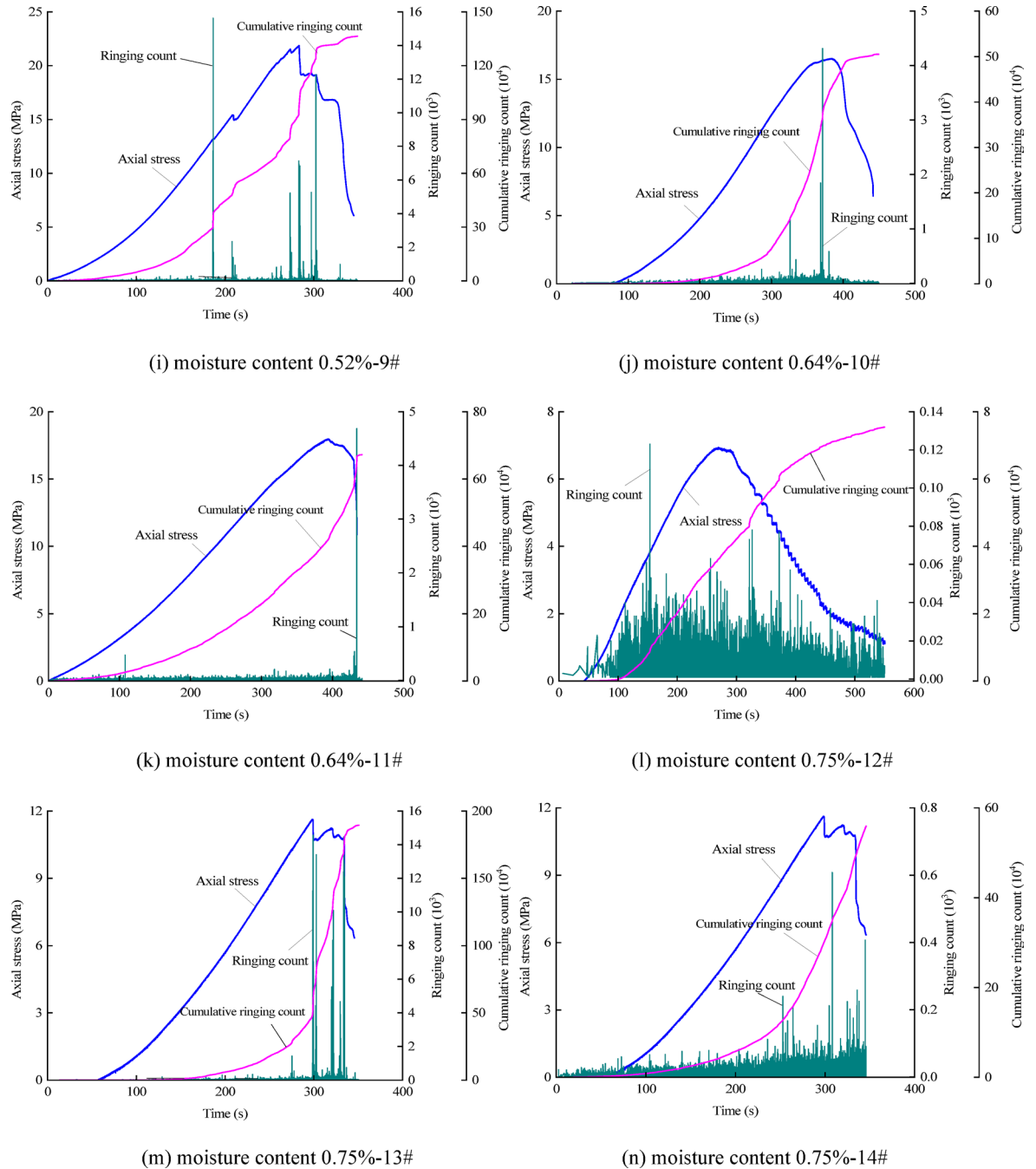


Fig. 7. (continued)

Energy storage, absorption, and dissipation characteristics

According to Eq. (2) to (5), process the experimental data and plot the energy axial compression relationship curve of each water containing coal sample during uniaxial compression, as shown in Fig. 9.

It can be seen from Fig. 9 that under different moisture content conditions, the energy-axial strain relationship curves of each coal sample show similar change laws, which can be specifically divided into the following stages: (1) Primary crack compaction and closure stage: At the initial stage of loading, as the axial pressure increases, the total energy absorbed by the coal sample and the releasable elastic energy show an upward concave change trend. At this time, part of the energy absorbed by the coal sample is converted into releasable elastic energy, and the other part is used for the compaction and closure of primary pores and cracks, and then dissipated. This stage is characterized by relatively little energy absorbed by the sample and releasable elastic energy, but relatively more dissipated energy. (2) Linear elastic stage: With the further increase of axial pressure, the slope of the curve of total energy absorbed by the coal sample versus axial pressure and the slope of the curve of releasable elastic energy versus axial pressure both gradually increase. The testing machine continues to do work on the sample, so that the energy absorbed by the sample and the releasable elastic energy keep increasing, but

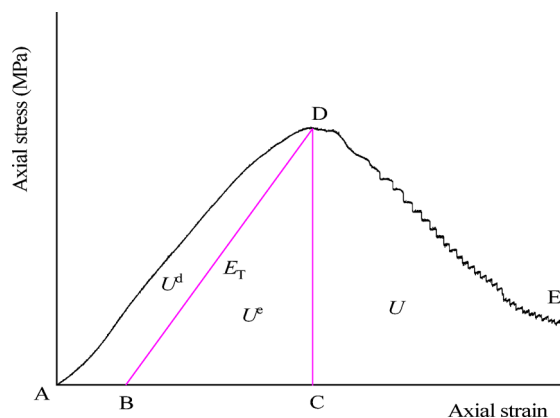


Fig. 8. Relationship curve between dissipated energy and releasable elastic energy during uniaxial compression.

the change rate of dissipated energy is small. At this stage, the energy absorbed and stored by the coal sample and the releasable energy are relatively high, while the dissipated energy is relatively low. (3) Plastic deformation stage: When the axial pressure continues to be loaded, a large number of new microcracks will be generated, expanded, evolved and gradually connected inside the coal sample, and the sample will show obvious plastic deformation. In this process, the coal sample continues to store energy, and the increase rates of absorbed stored energy and dissipated energy also continue to rise. (4) Post-peak deformation and failure stage: When the axial pressure reaches the limit value that the sample can bear, the sample enters the post-peak deformation and failure stage, and a macroscopic through-fracture surface will be formed. Although the sample can still absorb a small amount of energy from the outside when sliding along the fracture, the rate of total energy absorption slows down significantly. At the same time, the stress is released, the releasable elastic energy decreases rapidly, and the dissipated energy increases rapidly. The energy values at the peak of water-bearing coal samples are extracted, as shown in Table 3.

It can be seen from Table 3 that in the dry state, the total pre-peak absorbed energy of the coal samples ranges from 0.154 to 0.215 MJ/m³, with an average of 0.184 MJ/m³; the releasable elastic energy at the peak ranges from 0.125 to 0.193 MJ/m³, with an average of 0.159 MJ/m³. When the moisture content is 0.25%, the total pre-peak absorbed energy of the coal samples is between 0.111 and 0.129 MJ/m³, with an average of 0.120 MJ/m³; the releasable elastic energy at the peak is in the range of 0.101–0.115 MJ/m³, with an average of 0.108 MJ/m³. At a moisture content of 0.30%, the total pre-peak absorbed energy of the coal samples ranges from 0.080 to 0.092 MJ/m³, averaging 0.087 MJ/m³; the releasable elastic energy at the peak is between 0.059 and 0.072 MJ/m³, with an average of 0.065 MJ/m³. When the moisture content is 0.52%, the total pre-peak absorbed energy of the coal samples is 0.088–0.1022 MJ/m³, with an average of 0.095 MJ/m³; the releasable elastic energy at the peak is 0.070–0.086 MJ/m³, averaging 0.078 MJ/m³. At a moisture content of 0.64%, the total pre-peak absorbed energy of the coal samples ranges from 0.059 to 0.082 MJ/m³, with an average of 0.071 MJ/m³; the releasable elastic energy at the peak is between 0.048 and 0.070 MJ/m³, averaging 0.059 MJ/m³. When the moisture content is 0.75%, the total pre-peak absorbed energy of the coal samples is 0.028–0.042 MJ/m³, with an average of 0.033 MJ/m³; the releasable elastic energy at the peak is 0.025–0.036 MJ/m³, averaging 0.029 MJ/m³. It can be concluded that during the loading process of the coal samples, only a small part of the total absorbed energy is stored in the samples in the form of releasable elastic energy, while most of the total energy is dissipated by the compaction of various internal defects in the samples, as well as the new microcracks generated during the sliding and yielding stages. After reaching the peak, the releasable elastic energy can promote the expansion, penetration, and sliding of new cracks inside the samples until the samples completely lose their bearing capacity.

The curves depicting the variation of total energy and releasable elastic energy at the peak stress point of coal samples with moisture content are shown in Fig. 10. It can be observed that both the total absorbed energy and the releasable elastic energy before the peak decrease with increasing moisture content, following an overall quadratic functional decline. This reduction occurs because water fills the internal structure (pores and fractures) of the coal samples, thereby weakening their energy absorption capacity prior to reaching peak stress and simultaneously reducing the stored releasable elastic energy.

Analysis and discussion of water-induced mechanisms

The experimental results of this study demonstrate that water intrusion significantly reduces the strength and elastic modulus of coal samples and alters their acoustic emission activity and energy evolution characteristics. These macroscopic phenomena originate from a series of internal physicochemical interactions triggered by water molecules penetrating the coal matrix, primarily manifested in the following two aspects:

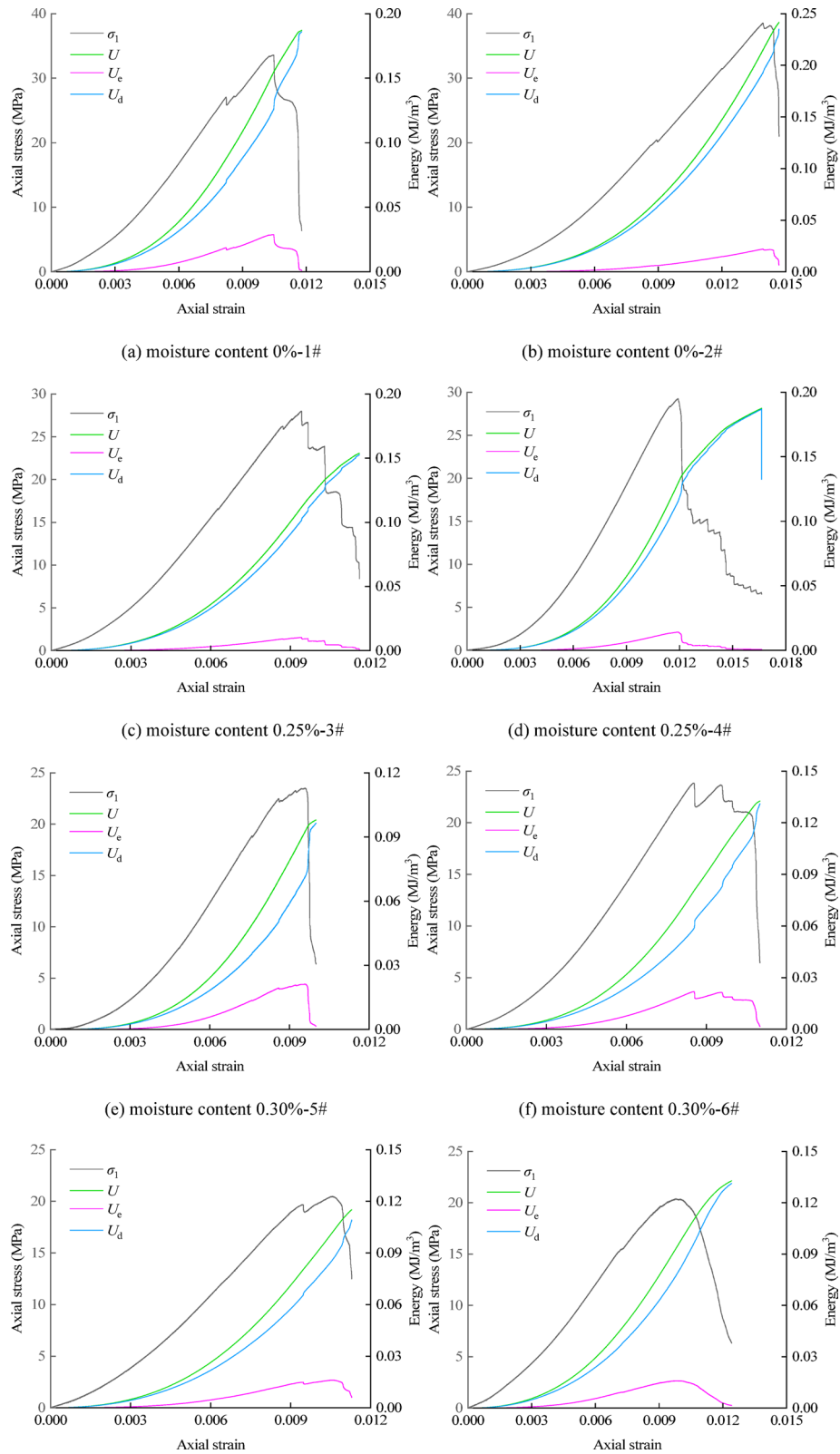


Fig. 9. Relationship curves of axial stress-axial strain-energy of each water-bearing coal sample.

Mechanical effect of pore water pressure

After water molecules enter the complex pore and fracture network of the coal, pore water pressure is generated. According to the principle of effective stress³¹, the effective stress σ' acting on the coal sample can be expressed as:

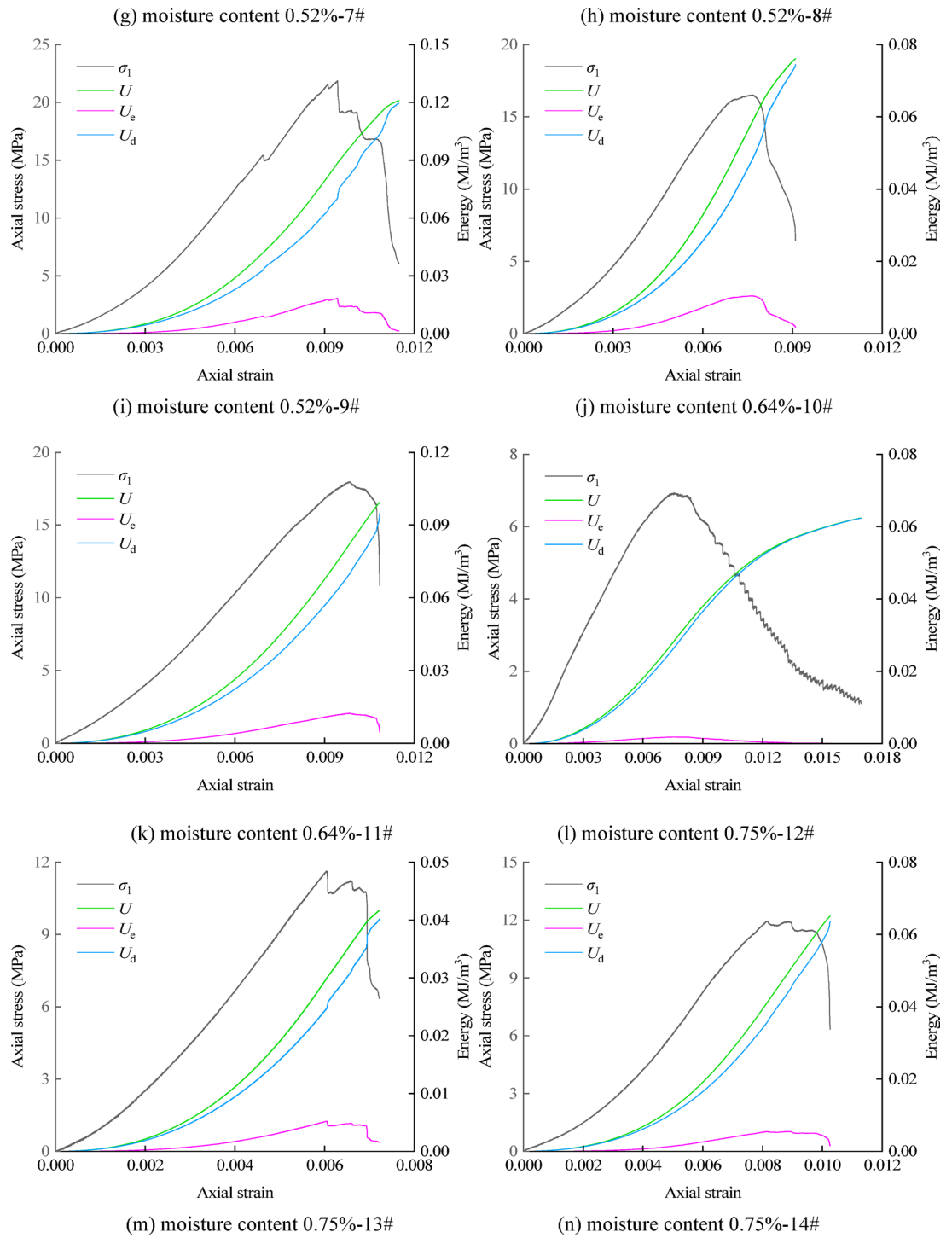


Fig. 9. (continued)

$$\sigma' = \sigma - p \tag{6}$$

where σ is the total stress and p is the pore water pressure.

During uniaxial compression, the total stress σ applied by the external load remains constant. The presence of pore water pressure p offsets a portion of the effective stress, directly reducing the compressive force and frictional resistance between coal particles. As a result, the coal sample reaches its yield and failure conditions under lower macroscopic loads, manifesting as a reduction in peak strength. Furthermore, the “cushioning” effect of pore water pressure mitigates stress concentration at crack tips^{12,15,32}, delaying the initiation and stable propagation of microcracks. This may explain the relatively lower acoustic emission activity observed in water-bearing coal samples during the elastic stage (Fig. 7).

Moisture content/%	No.	U(MJ/m ³)	U _c (MJ/m ³)	U _d (MJ/m ³)	U _c /U(%)	U _d /U(%)
0	1#	0.154	0.029	0.125	18.73%	81.27%
	2#	0.215	0.022	0.193	10.23%	89.77%
0.25	3#	0.111	0.010	0.101	9.24%	90.76%
	4#	0.129	0.014	0.115	10.97%	89.03%
0.30	5#	0.093	0.021	0.072	22.87%	77.13%
	6#	0.080	0.022	0.059	27.14%	72.86%
0.52	7#	0.102	0.016	0.086	15.74%	84.26%
	8#	0.093	0.016	0.077	17.10%	82.90%
	9#	0.088	0.018	0.070	20.74%	79.26%
0.64	10#	0.059	0.010	0.048	17.76%	82.24%
	11#	0.082	0.012	0.070	15.10%	84.90%
0.75	12#	0.028	0.002	0.027	6.51%	93.49%
	13#	0.030	0.005	0.025	17.42%	82.58%
	14#	0.041	0.005	0.036	13.24%	86.76%

Table 3. Energy parameters at the peak of each water-bearing coal sample.

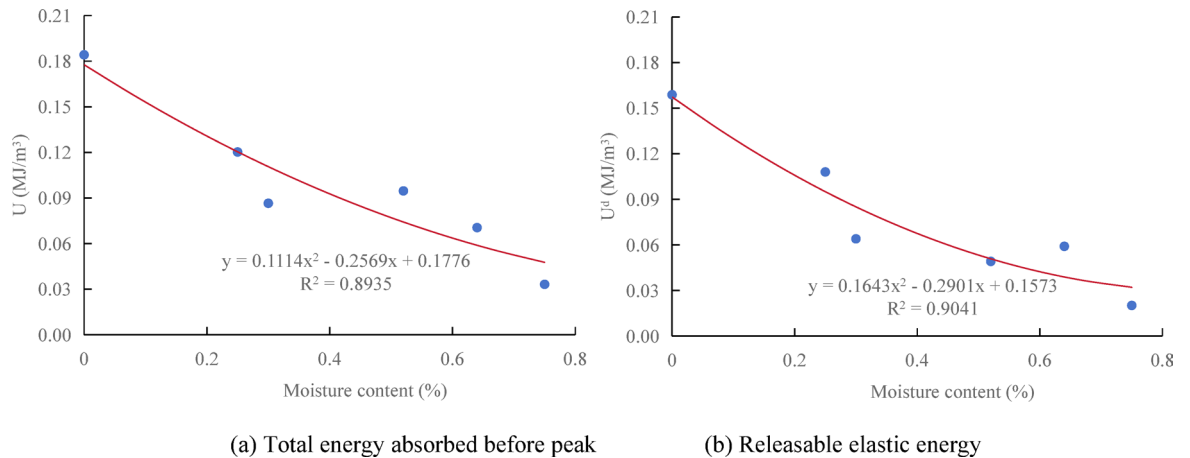


Fig. 10. Relationship curve between total absorbed energy, releasable elastic energy and moisture content pre-peak.

Structural degradation effect of water-rock interaction

This is the fundamental cause of the intrinsic weakening of coal strength, mainly involving physical softening and chemical corrosion:

Physical softening and lubrication: Water, being a highly polar molecule, is readily adsorbed by clay minerals (e.g., kaolinite, montmorillonite) and coal matrix surfaces. This adsorbed water film significantly weakens the cementation between mineral particles and acts as a lubricant, reducing the internal friction coefficient¹². Consequently, particles are more prone to slip under shear stress, macroscopically exhibiting enhanced plastic deformation in coal samples and a transition from brittle to ductile failure modes, along with a notable decrease in peak strength.

Chemical corrosion and dissolution: Water, especially when containing acidic ions (e.g., CO₃²⁻, SO₄²⁻) commonly found in groundwater environments, reacts with soluble cementing materials in coal (such as carbonate minerals like calcite and dolomite), leading to their dissolution and loss¹⁷. This corrosion directly damages the cementation structure supporting the coal matrix, causing irreversible damage. The prolonged chemical corrosion observed with increasing immersion time aligns well with the experimental results showing a continuous decrease in coal strength (Fig. 5) and an increase in the softening coefficient (Fig. 6).

Water wedge effect: Driven by capillary forces, water molecules penetrate the tips of microcracks in the coal, generating tensile stress (water wedge effect). This promotes the further propagation and interconnection of microcracks, exacerbating the initial damage in the coal matrix.

Correlation between mechanisms and macroscopic responses

The combined action of the above two mechanisms explains the macroscopic observations of this study:

Strength and modulus degradation: Pore water pressure reduces effective stress, while water-rock interactions weaken cementation and friction, collectively leading to a decline in macroscopic strength and stiffness.

Changes in acoustic emission characteristics: Water suppresses the generation of early microcracks (evidenced by a distinct quiet period) while promoting the concentrated formation of macroscopic failure surfaces later, resulting in more intense and clustered acoustic emission signals during failure.

Energy evolution properties: Due to pre-weakening of the internal structure, water-bearing coal samples accumulate significantly less releasable elastic strain energy (U_e) before failure (Table 3). More input energy is consumed as dissipated energy (U_d) during compaction and plastic deformation, overcoming water film lubrication and particle slip rather than being stored for brittle fracture. This is consistent with their ductile failure characteristics.

Conclusions

This study selects the Wuzu coal in Pingmei 11 Mine as the research object. The coal samples were subjected to water immersion treatment, followed by uniaxial compression and acoustic emission tests on the water-bearing coal samples. The strength, deformation, acoustic emission, and energy characteristics of the raw coal samples under water-force coupling were analyzed. The conclusions are as follows:

(1) The stress-strain curves of the water-bearing coal samples exhibit similar variation characteristics, showing stages of crack compression, linear elasticity, plastic deformation, and post-peak failure. As the water content increases, the failure characteristics of the coal samples transition from brittle to ductile.

(2) Water weakens the mechanical parameters of the raw coal. The uniaxial compressive strength, elastic modulus, deformation modulus, and peak strength of the coal samples decrease quadratically with increasing water content. The softening coefficient of the coal samples increases quadratically with both rising water content and prolonged immersion time.

(3) During the first two stages of the stress-strain curve (crack compression and linear elasticity), the acoustic emission signals are relatively sparse. As the coal samples enter the plastic deformation stage, the acoustic emission signals gradually increase. When the samples approach failure and beyond, the acoustic emission signals rise sharply.

(4) Based on energy characteristic analysis during uniaxial compression, the storage, absorption, and dissipation properties of the water-bearing coal samples were evaluated. The total absorbed energy and releasable elastic energy before the peak decrease quadratically with increasing water content. This is attributed to water filling the internal structures (pores and cracks) of the coal samples, reducing their energy absorption capacity before peak stress and simultaneously diminishing the stored releasable elastic energy.

Data availability

The datasets generated or analyzed during the current study are available from the corresponding author on reasonable request.

Received: 11 August 2025; Accepted: 7 October 2025

Published online: 13 November 2025

References

- Wu, Q., Qian, Z. J., Dong, D. L., Song, E. C. & Hong, Y. Q. Forming mechanism and prevention of water-coal-burst disaster on extremely inclined faces under ordovician aquifer. *J. China Coal Soc.* **25** (04), 408–411 (2000).
- Wang, B. et al. Coupling effect of water-rock in the process of coalbed methane extraction and its response to production capacity -Fanzhuang block in Qinshui basin as an example. *J. China Coal Soc.* **50** (08), 4008–4021 (2025).
- Pang, Z. Z. et al. Theory and engineering practice of coal-water coordinated mining based on constraints of formation bearing capacity. *Coal Geol. Explor.* **53** (07), 1–11 (2025).
- Yang, H. et al. Fractal characteristics of effective seepage channel structure of water infusion coal based on NMR experiment. *Rock. Soil. Mech.* **41** (04), 1279–1286 (2020).
- Wang, G. et al. Research on mechanism and engineering application of coal seam water injection to mine disaster prevention. *J. Shandong Univ. Sci. Technol. (Natural Science)*. **44** (03), 1–12 (2025).
- Yang, M. et al. Study on the dynamic evolution of coal pore under variable pressure water injection environment. *J. China Coal Soc.* **49** (S2), 1033–1040 (2024).
- Wang, L. M., Luo, Y. H. & Bai, H. X. Chemical regulation of coal microstructure and study of water injection displacement gas law. *J. China Coal Soc.* **48** (08), 3091–3101 (2023).
- Zhang, J. J., Yuan, X. L., Zhang, H. Q., Chen, Y., Han, G. Q. & Nian, G. X. Study on the effect of moisture on mechanical properties and impact energy index of coal. *Safety in Coal Mines* **54** (7), 26–33 (2023).
- Yang, K., Wei, Z., Dou, L. T. & Chi, X. L. Research on dynamic tensile energy evolution and fractal characteristics of water-bearing coal samples. *J. China Coal Soc.* **46** (2), 398–411 (2021).
- Zhang, M. B., Zhu, H. Q., Li, M. Q., Zhou, D. H. & Li, W. Effect of moisture content on damage deformation of coal containing gas under loading and unloading conditions. *J. Saf. Sci. Technol.* **13** (05), 90–95 (2017).
- Wang, B. F., Wu, L., Zhang, J., Liang, B. & Liu, B. C. Experiment on size effect of coal and rock deformation characteristics in coalmine underground reservoir. *J. Min. Saf. Eng.* **38** (04), 810–818 (2021).
- Li, B. B., Wang, Z. H., Ren, C. H., Zhang, Y., Li, J. H. & J. X., and Mechanical properties and damage constitutive model of coal under the coupled hydro-mechanical effect. *Rock. Soil. Mech.* **42** (02), 315–323 (2021).
- Yao, Q. L., Yao, W. N., Li, X. H. & Tang, C. J. Study of mechanical properties and acoustic emission characteristics of coal measures under water-rock interaction. *J. China Univ. Min. Technol.* **50** (03), 558–569 (2021).
- Duan, S. L. et al. Permeability evolution of water-bearing coal considering dynamic slippage effect. *Chin. J. High. Press. Phys.* **41** (04), 798–808 (2022).
- Yin, D. W. et al. Experimental study on mechanical properties of coal soaked in pressurized water considering initial damage. *J. China Coal Soc.* **48** (12), 4417–4432 (2023).
- Yin, D. W., Sun, P. X., Tan, H. H. Y., Qu, X., Wang, F., & Jiang, N. Characterization of damage deterioration of pressure waterlogged coal rock under cyclic loading and unloading effects. *J. China Coal Soc.* 1–17 (2025).
- Chen, J. H., Wang, S. J., Zhang, H., Hu, S. S. & Zhang, P. L. J. W. Corrosion characteristics and dynamic properties of the coal-rock combination under hydrochemical condition. *J. China Univ. Min. Technol.* **52** (05), 952–962 (2023).

18. Chen, G. B., Li, Y., Li, T., Zhang, J. W. & Zhang, G. H. Mechanical response and deterioration mechanism of coal-rock combined body under the action of Circulating water-rock. *J. Eng. Geol.* **32** (01), 108–119 (2024).
19. Lyu, K. et al. Deterioration of compressive properties of coal rocks under water and gas coupling. *J. Cent. South. Univ.* **31** (02), 477–495 (2024).
20. Gao, M. Z. et al. Macroscopic and microscopic mechanical behavior and seepage characteristics of coal under hydro-mechanical coupling. *J. Cent. South. Univ.* **31** (08), 2765–2779 (2024).
21. Qi, X. H. et al. Study on mechanical and seepage characteristics of liquid nitrogen freeze-thaw coal with different water content. *Chinese Q. Mech.* **45** (03), 808–824 (2024).
22. Qi, X. H., Zhang, Y., Hou, S. R., Tian, N. & Lv, Q. Enhancement mechanisms of coal permeability under water saturated conditions using liquid nitrogen freeze thaw cycles. *Sci. Rep.* **15**, 25178 (2025).
23. Li, S. W., Gao, M. Z., Li, Y. X., Wang, J. & Zeng, G. Effect of water on dynamic mechanical properties of coal under different depth stress conditions. *J. Cent. South. Univ.* **32** (01), 220–228 (2025).
24. Ma, Y. K., Zhang, Z. R. & Zhang, J. H. Experimental study on failure law and acoustic emission response of coal and rock under the action of water coupling and high pressure air impact. *J. Vib. Shock.* **44** (02), 1–10 (2025).
25. Pi, Z. K. et al. Experimental investigation into the impact of Cyclic high low pressure water immersion on the pore structure and mechanical properties of coal. *Sci. Rep.* **15**, 1288 (2025).
26. Feng, R. J., Zhu, Y. J., Deng, F. & He, J. Damage and breakage characteristics of loaded coal impacted by high-pressure pulse water jet and its influence factors. *Chin. J. High. Press. Phys.* **39** (03), 60–73 (2000).
27. Feng, R. J., Zhu, Y. J. & He, J. X. Damage and failure characteristics and influence analysis of heterogeneous loaded coal rock impacted by pulsed water jet. *J. Saf. Sci. Technol.* **21** (02), 90–98 (2025).
28. Hadizadeh, J. & Law, R. D. Water-weakening of sandstone and quartzite deformed at various stress and strain rates. *Int. J. Rock. Mech. Min. Sci. Geomech. Abstracts.* **28** (5), 431–439 (1991).
29. Li, B. B. et al. Study on damage-energy evolution characteristics of coal under triaxial stress, China Safety Science Journal. **29**(10): 98–104 (2019).
30. Shan, P. F., Lai, X. P., Cui, F. & Cao, J. T. Energy dissipation properties and mechanisms of fractured coal-rock mass failure under mining condition. *J. Min. Saf. Eng.* **35** (04), 834–842 (2018).
31. Terzaghi, K. Die berechnung der durchlässigkeitsziffer des tones Aus dem Verlauf der hydrodynamischen spannungserscheinungen. *Sitzungsberichte Der Akademien Der Wissenschaften Wien Mathematisch-Naturwissenschaftliche Klasse Part. Ila.* **132** (3/4), 125–138 (1923).
32. Brace, W. F. & Martin, R. J. A test of the law of effective stress for crystalline rocks of low porosity. *Int. J. Rock Mech. Min. Sci.* **5** (5), 415–426 (1968).

Author contributions

J.W.: Conceptualization, Data curation, Investigation, Methodology, Original draft. F.X.: Methodology, Resources; Supervision, Review & editing (equal). Y.Y.: Investigation.

Funding

This study was sponsored by the Suzhou City University National-Level Pre-research Project (No.2024SGY017), Youth Science Fund Project of the National Natural Science Foundation of China (No.51804129), and Jiangsu Postdoctoral Research Funding Program (No.2019K139).

Declarations

Competing interests

The authors declare no competing interests.

Additional information

Correspondence and requests for materials should be addressed to F.X.

Reprints and permissions information is available at www.nature.com/reprints.

Publisher's note Springer Nature remains neutral with regard to jurisdictional claims in published maps and institutional affiliations.

Open Access This article is licensed under a Creative Commons Attribution-NonCommercial-NoDerivatives 4.0 International License, which permits any non-commercial use, sharing, distribution and reproduction in any medium or format, as long as you give appropriate credit to the original author(s) and the source, provide a link to the Creative Commons licence, and indicate if you modified the licensed material. You do not have permission under this licence to share adapted material derived from this article or parts of it. The images or other third party material in this article are included in the article's Creative Commons licence, unless indicated otherwise in a credit line to the material. If material is not included in the article's Creative Commons licence and your intended use is not permitted by statutory regulation or exceeds the permitted use, you will need to obtain permission directly from the copyright holder. To view a copy of this licence, visit <http://creativecommons.org/licenses/by-nc-nd/4.0/>.

© The Author(s) 2025